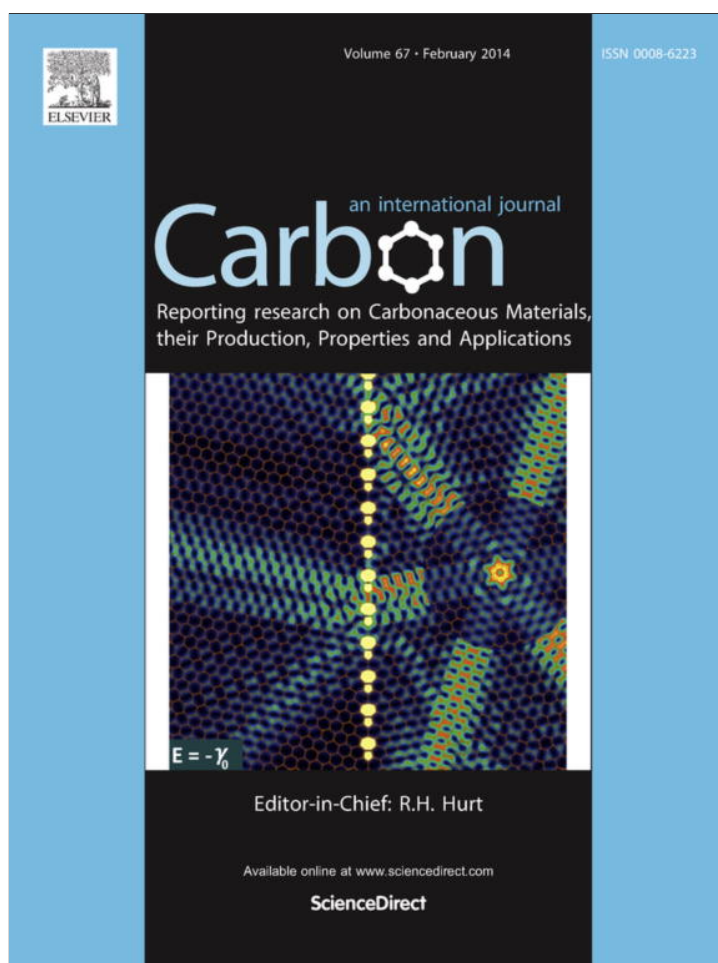


Provided for non-commercial research and education use.
Not for reproduction, distribution or commercial use.



This article appeared in a journal published by Elsevier. The attached copy is furnished to the author for internal non-commercial research and education use, including for instruction at the authors institution and sharing with colleagues.

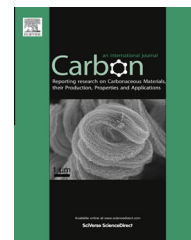
Other uses, including reproduction and distribution, or selling or licensing copies, or posting to personal, institutional or third party websites are prohibited.

In most cases authors are permitted to post their version of the article (e.g. in Word or Tex form) to their personal website or institutional repository. Authors requiring further information regarding Elsevier's archiving and manuscript policies are encouraged to visit:

<http://www.elsevier.com/authorsrights>

Available at www.sciencedirect.com

ScienceDirect

journal homepage: www.elsevier.com/locate/carbon

Hydroxyapatite/graphene-nanosheet composite coatings deposited by vacuum cold spraying for biomedical applications: Inherited nanostructures and enhanced properties



Yi Liu ^a, Zhaohui Dang ^b, Yuyue Wang ^b, Jing Huang ^a, Hua Li ^{a,*}

^a Key Laboratory of Marine Materials and Related Technologies, Ningbo Institute of Materials Technology and Engineering, Chinese Academy of Sciences, Ningbo 315201, China

^b State Key Laboratory for Mechanical Behavior of Materials, Xi'an Jiaotong University, Shaanxi 710049, China

ARTICLE INFO

Article history:

Received 24 July 2013

Accepted 28 September 2013

Available online 9 October 2013

ABSTRACT

Recent exciting findings of the biological interactions of graphene materials have shed light on potential biomedical applications of graphene-containing composites. Fabrication of bulk composites in particular nanostructured coatings from nanosize particles/sheets yet remains elusive. Here we report hydroxyapatite (HA) and HA-graphene nanosheet (GN) composites synthesized by liquid precipitation approach and following coating deposition by vacuum cold spraying. The HA-GN composite coatings retained intact nano-structural features of both HA and GN. The impact of the HA-GN particles during coating formation created layered coating structures and mechanical interlocking was achieved by even distribution of GN. *In vitro* cell culture assessment showed that filopodia of osteoblast cells inclined to move towards and got anchored by GN. Further observation by electron microscopy of adsorption of fibronectin on GN by negative staining showed fast adsorption of fibronectin in unfolded shape with the length of ~100–135 nm. This presumably accounts for the enhanced spreading and subsequent proliferation of the cells on the GN-containing coatings. The strategy of depositing the novel HA-GN composite coatings gives bright insight into potential biomedical applications of the composites.

© 2013 Elsevier Ltd. All rights reserved.

1. Introduction

Research in biomaterials has been booming in recent decades. Development of novel biomaterials holds the priority among the extensive worldwide efforts devoted to biomedical engineering. The biomaterials for orthopedic surgery usually encounter complex service environments, requiring versatile performances of the materials. As one of the major players for orthopedic surgery, hydroxyapatite (HA) has been developed in response to the deficient biocompatibility of alloys,

e.g. stainless steel, Co-based alloy, Ti and Ti-6Al-4V, which usually lose their proper function in a long term due to degradation from wear, disease, or injury [1–3] or tendency to release metallic ions leading to a high potential to corrode in the biological environments [4,5]. Yet, regardless of the successful application of HA in orthopedic surgery for promoting fast fixation of bony tissues, there are still concerns related to its long-term performance, i.e., the intrinsic brittleness and low fracture toughness of HA [6–8]. Mechanical performances of HA could be improved by incorporating second phase

* Corresponding author. Fax: +86 574 86685159.

E-mail address: lihua@nimte.ac.cn (H. Li).

0008-6223/\$ - see front matter © 2013 Elsevier Ltd. All rights reserved.

<http://dx.doi.org/10.1016/j.carbon.2013.09.088>

reinforcements like ethylene-based polymer, Ti-alloys, alumina, yttria-stabilized zirconia, carbon nanotube etc. [9–13]. However, few materials that have been considered for HA-based composites satisfy both favorable biocompatibility and sufficient strength. As an alternative novel material, graphene has been attracting intense attentions due to its unique structural features and exceptional mechanical properties [14–17]. Exciting findings of the biological performances of graphene reported in recent years [18–20] further imply the possibility of it being used as additives in HA for load-bearing biomedical applications, even though the reason for exceptional biocompatibility of graphene remains obscure.

It is essential that any biomaterials that are implanted in the body must operate in powder or bulk form. Employment of biocompatible materials like HA as coatings on bioinert metallic implants is the key for their long term functional services [21–23]. This consequently raises the concerns of selecting appropriate techniques for depositing the coatings. Among the approaches used nowadays, of particular interest is the thermal spray technology, which offers advantages of cost-effective and environment-friendly production, controllable microstructure and good properties of the coatings [24–27]. Thermal sprayed HA and HA-based composites have been successfully used in clinical surgery [3,22]. It is well established that microstructure, crystallinity, and phase composition of HA coatings are critical in deciding behaviors of the cells attached/proliferated on them [3,25–27]. Nanostructured HA exhibit further enhanced biocompatibility when compared to their conventional counterparts [28–32]. This enhanced biocompatibility is translated into better adhesion and higher reproduction of the cells on the surfaces of these materials, which is very important indication of improved bio-performances of the implants. In this regard, searching pertinent process for fabricating nanostructured biomedical coatings has been one of the major research goals in recent years. Thermal spray process is usually intrinsically associated with melting of feedstock powder, without which it is extremely difficult to make fine coatings. Certain degree of melting is usually necessary for attaining a sufficient level of particle adhesion and cohesion. To deposit coatings from nano particles, the often used agglomeration by spray-drying processing of the particles [33] introduces complexity and difficulties in controlling coating structures. Vacuum cold spray (VCS), a method based on shock-loading solidification [34,35], is a novel and promising spray technique which enables deposition of powder with particle size range of 0.02–2 μm at room temperature on various substrates. VCS is of particular prospect for spraying nanosized particles with high deposition efficiency in coating thickness ranging from several to tens of microns per minute [34–37].

In this paper, we report novel nano-HA/graphene-nanosheet (GN) composite coatings deposited by VCS, giving insights into their potential biomedical applications for repair/replacement of hard tissues. To elucidate the performances of the nanostructured coatings, we performed microstructural characterization and *in vitro* cell culture test. The biocompatibility of GN was further investigated by assessing the adsorption of fibronectin by electron microscopy. This study provides a competitive approach for processing nanostructured biomedical materials.

2. Materials and methods

2.1. Synthesis of graphene and HA-graphene composite powder

Large-scale GN was chemically fabricated from high purity flakey graphite. HA powder in nanosizes was synthesized by the wet chemical approach using stoichiometric reaction between $(\text{NH}_4)_2\text{HPO}_4$, $\text{Ca}(\text{NO}_3)_2$, and $\text{NH}_3\cdot\text{H}_2\text{O}$. Microstructural characterization revealed that HA grains had the size of ~ 20 – 45 nm in length and ~ 10 nm in diameter. HA-GN composites were produced by adding GN to the solution prior to the synthesis of HA. The detailed procedures have been reported in another paper [38].

2.2. Deposition of HA-GN coatings

HA coatings with/without addition of graphene platelets have been vacuum cold sprayed onto Ti substrates at room temperature. The VCS process was carried out using VCS-2000 system (developed by Xi'an Jiaotong University, China). The VCS system consists of a vacuum deposition chamber, a set of vacuum pumps, an aerosol generation room, an accelerating carrier gas unit, a vibration system to mix the powder with the carrier gas, and a control unit. The VCS system has been schematically depicted in Fig. 1d. The deposition chamber contains a micron-sized nozzle, a substrate holder and a two-dimensional worktable. A rotary vane vacuum pump coupled to a mechanical booster was used to pump down the chamber to a pressure of 100–5000 Pa during spraying. Helium gas with the flow rate of 5 l/min was used for feeding and accelerating the powder particles. The ultrafine powder was mixed with and accelerated by the helium gas to form an aerosol flow which was further accelerated by carrier gas through the micro-orifice nozzle (Laval cavity design). The specially designed powder feeding system favors easy formation of aerosol flow for the nano-/submicron-sized powder. The scanning speed of 10 mm/s and the spray distance of 10 mm were adopted for the coating deposition.

2.3. Microstructure characterization and property evaluation

Microstructure of the powder and the coatings was characterized by transmission electron microscopy (TEM, FEI Tecnai F20, the Netherlands) and field emission scanning electron microscopy (FESEM, FEI Quanta FEG250, the Netherlands). For the TEM characterization, the specimen preparation involved transferring the powder suspension in ethanol onto micro grids and letting the solvent evaporate. GN was also characterized by atomic force/scanning tunneling microscopy (AFM/STM, Dimension 3100V, Veeco, USA). The suspension that contained graphene platelets encountered sonication before it was deposited onto polished silicon wafer for subsequent AFM measurement. Phase composition of the samples was analyzed by X-ray diffraction (XRD, D8 Advance, Bruker AXS, Germany) using $\text{Cu K}\alpha$ radiation ($\lambda = 1.5406 \text{ \AA}$) operated at 40 kV and 40 mA. The goniometer was set at a scan rate of $0.033^\circ/\text{s}$ over a 2θ range of 20 – 60° . Adhesive strength of the HA and HA-GN coatings on Ti substrates was assessed through scratch test conducted using a

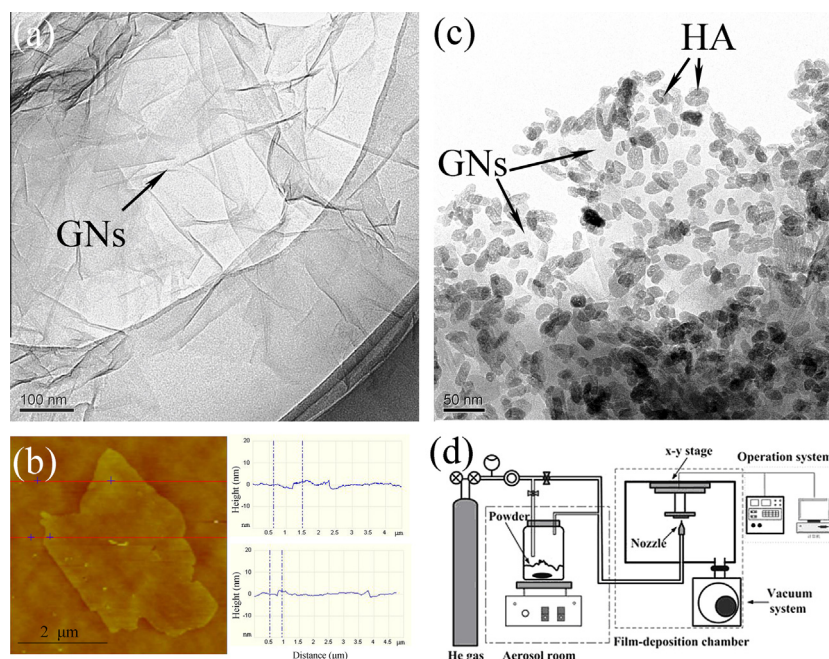


Fig. 1 – Characterization of the synthesized GN and HA–GN composite powder (a–c) and schematic depiction of the VCS system [37] (d), (a) TEM image of the GN showing wrinkled-paper-like morphology, (b) AFM analysis showing uniform height of 0.8–1.1 nm and the lateral dimensions ranging from a few hundred nanometers to $\sim 4 \mu\text{m}$ of GN, typical line profiles taken along the marked red lines are also presented superimposed on the image, and (c) TEM image of the HA–GN powder showing rod-like HA nano grains evenly attaching on graphene flakes with an intimate contact. (A colour version of this figure can be viewed online.)

micro-scratch tester (MST, WS-2005, China). In the MST process, when the diamond drill bit scratched the coating, the acoustic signal was acquired for estimating the adhesion. Five replicates of each sample were tested. Specific surface areas of the samples were measured using the Brunauer, Emmett, and Teller (BET) method by adsorption of nitrogen gas on ASAP 2020 M apparatus operated at 77.3 K. The BET surface area was calculated over the relative pressure range of 0.05–0.20 MPa. Fracture toughness (K_{Ic}) of the coatings was determined by using the indentation approach. The test was conducted on Micro-Vickers microhardness tester (HV-1000, Shanghai Lianer Testing Equipment Corporation, China). 300 gf Vickers load was applied on polished cross-sections of the coatings with a loading time of 10 s. A total of 10 points were collected for each sample. The fracture toughness was calculated by using the Anstis equation [39]: $K_{Ic} = 0.016(E/H)^{1/2}(P/C)^{3/2}$, where P is the indentation load, C is the length of the crack caused by the indentation, H is the microhardness, and E is the elastic modulus. The microhardness and elastic modulus of the coatings were derived from the loading–unloading curves in nano-indentation test conducted using a standard Berkovich indenter on nanomechanical test system (NANO G200, MTS, USA). The maximum indentation depth chosen for the present test was 1 μm . Six indentations were made for each test on each sample.

2.4. Cell culture test

Attachment and proliferation of the human osteoblast cells (HFOB 1.19 SV40 transfected osteoblasts) on the Ti, HA and

HA–GN coatings were examined. Prior to the *in vitro* experiments, the cells were cultured in α -minimum essential medium (α -MEM) (SH30265.01B, HyClone, USA) supplemented with 10% heat-inactivated fetal bovine serum, 100 U/ml penicillin and 100 $\mu\text{g}/\text{ml}$ streptomycin in an atmosphere of 100% humidity and 5% CO_2 at 37 $^\circ\text{C}$. The osteoblasts were seeded at a density of 2000 cells/ cm^2 onto the samples in 24-well plates with 2 ml media being contained in each well and grew under standard culture conditions (100% humidity and 5% CO_2 at 37 $^\circ\text{C}$) for 3 h, 1 day, 3 days, and 5 days. Prior to seeding, the samples were autoclave sterilized for 30 min. For FESEM observation of the cells attaching on the surfaces of the samples, the cells after incubation were fixed in 2.5% glutaraldehyde for 24 h, dehydrated gradually and coated with Pt. Three samples were tested for each type of the specimens. Proliferation of the cells was analyzed using the methyl thiazole tetrazodium (MTT) assay. The MTT stock solution of 5 mg/ml (Sigma, St Louis, MO, USA) was prepared by dissolving MTT in phosphate buffered saline (PBS), filtered through a 0.2 μm filter and stored at 4 $^\circ\text{C}$. The MTT solution was prepared as per the standard protocol provided by the supplier and was read using 490 nm wavelength on a microplate reader machine (Spectra Max 190, MD, USA). For each type of the specimens, three samples were tested to get an average value and each sample was read for three times. Differentiation of the cells cultured on the samples was assessed by measuring their alkaline phosphatase (ALP) activity. The cells (1×10^4 cells/ml) were seeded on the specimens and cultured for 7 days. They were washed twice with PBS and lysed by three cycles of freezing and thawing program. The as-received ali-

quots of supernatants were subjected to ALP activity and protein content measurement by using an ALP kit and a micro-Bradford assay kit (Nanjing Jiancheng Biological Engineering Institute, China). The absorbance of the reaction product, p-nitrophenol, was measured at the wavelength of 405 nm on the microplate reader machine. Paired student's *t*-distribution was employed to clarify the level of significance (*p*) in difference between two sets of data. Data was presented with standard deviation (\pm SD) and statistical significance was set at $p < 0.05$. For further disclosing the effect of the addition of GN on the biocompatibility of the coatings, adsorption behavior of fibronectin on GN was typically investigated by negative staining and TEM observation. As a cell adhesion protein, fibronectin is an ideal model protein for investigation in molecular level of biological responses to GN. For the negative-staining, the GN film was prepared by transferring GN dispersion in ethanol to TEM grids and letting the solvent evaporate at room temperature. A 5 μ l drop of fibronectin sample (Sigma, ref. F-0895) with the concentration of 50 μ g/mL in PBS was applied to the 300-mesh copper grid covered with a thin layer of GN. After removing the excess solution by blotting with filter paper, the sample grid was stained by using two 5 μ l drops of 2% (w/v) uranyl acetate solution. Excess stain was removed by blotting, and the grids were quickly dried by argon flow after final blotting. Images were recorded under low-dose conditions ($10 \text{ e}/\text{\AA}^2$) using a charge-coupled device camera in a field emission TEM operated at 200 kV at a magnification of 7100 \times and with an under-focus values varied from 1.0 to 1.5 μ m. Picking and image processing of individual particle images were made using the software package EMAN [40].

3. Results and discussion

3.1. Microstructure of the composite coatings

The as-synthesized GN shows wrinkled-paper-like morphology (Fig. 1a). AFM measurements suggest the uniform height of the nanosheet of 0.8–1.1 nm and the lateral dimensions ranging from a few hundred nanometers to $\sim 4 \mu$ m (Fig. 1b). In accordance with previous reports [15] and TEM observation [38], GN is interpreted to be single-layered sheets. Further TEM characterization reveals that rod-like HA nano grains evenly attach on graphene flakes with an intimate contact (Fig. 1c). HA grains have the size of ~ 20 –45 nm in length and ~ 10 nm in diameter.

Nanostructured HA and HA–GN coatings were successfully deposited by the VCS. FESEM views from top surfaces of the coatings (Fig. 2) suggest similar microstructural features for the coatings with/without addition of GN. The coatings demonstrate micron-sized pits and protrusions on their surfaces, indicating rebounding of certain amount of HA nano particles upon their impingement during coating formation stage, which is usual during cold spraying since cold sprayed coating is composed of accumulated individual particles accomplished by tamping effect [36,37,41]. It was acknowledged that surface roughness is critical in allowing the growth of cells because surfaces influence protein interaction, which decides subsequent cell adhesion [30,32]. The rough surfaces

of the HA–GN coatings might favor positive cell responses. As noticed from the close view of the coatings from their surfaces (Fig. 2), randomly oriented small HA crystallites in the size of < 20 nm can be clearly seen, which are identical to the starting rod-like HA feedstock. Graphene flakes are homogeneously dispersed in HA matrix in the coatings. The cross-sectional morphologies of the coatings show the thickness of up to 50 μ m (Fig. 2). Porous topographical structure can be clearly seen for the coatings, while the cross-sectional views suggest much dense structure. The average porosity of the coatings is 13.2%, 12.9%, and 8.7% for the pure HA coating, the HA-0.1 wt.%GN coating and the HA-1.0 wt.%GN coating, respectively. It is noted that the GN-containing coatings exhibit more remarkable layered structure (Figs. 2c-3 vs a-3), indicating unusual participation of GN in the shock loading formation of the coatings (the HA particles in nanosizes are unlikely responsible for the layered structure). GN in irregular curvature is clearly seen. Magnified view shown at the bottom of Fig. 2c-3 verifies the presence of GN, which solely accounts for the lamella coating structure. Strikingly, further examination also suggests that GN is the first layer that intimately contacts with the substrate, as indicated by the magnified coating-substrate interface shown at the top of Fig. 2c-3. This structural feature has also been evidenced by TEM characterization (Fig. 3d).

TEM observation of the HA-1.0 wt.%GN coating from its cross-section shows the typical structure of the area close to the coating/substrate interface (Fig. 3). The image acquired at HA-rich area suggests accumulation of individual HA nano particles in a compact manner and majority of HA retain their original nano features (Fig. 3a). Yet surprisingly, plastic deformation of certain amount of HA grains at their surrounding areas of contact is seen (Fig. 3a). Plastic deformation of sprayed particles is essential during cold spraying for strong adhesion and cohesion [34,35]. The phenomenon similar to cold welding has been previously revealed for cold sprayed coatings [42], which accounts for enhanced cohesion between individual particles. The shock loading-induced inelastic deformation presumably enhances interlocking for high adhesive/cohesive strength. In addition, well retained structural features of the HA–GN composites after the coating deposition are also seen (Fig. 3b), that is, the room-temperature VCS processing did not destroy the bonding between HA nano-rods and GN. This is further justified by the selected area electron diffraction (SAD) pattern (Fig. 3c), which is almost identical to that exhibited by the starting feedstock [38]. Based on these observations, the coating formation can be treated as accumulation of individual graphene sheets with nano HA grains intimately standing on them. While as shown in earlier part, GN used in this study has the thickness of 0.8–1.1 nm and the lateral dimensions ranging from a few hundred nanometers to $\sim 4 \mu$ m (Fig. 1). The coating formation is indeed not about deposition of individual nano HA particles nor individual GN, it is instead about accumulation of nano HA–GN slice. In fact, GN alone already achieved good bonding with the substrate (Fig. 3d). Deformation in terms of changes in curvature of GN in the coatings is inevitable (as seen in Fig. 2c-3), due mainly to the high speed impingement of the particles during the coating formation stage.

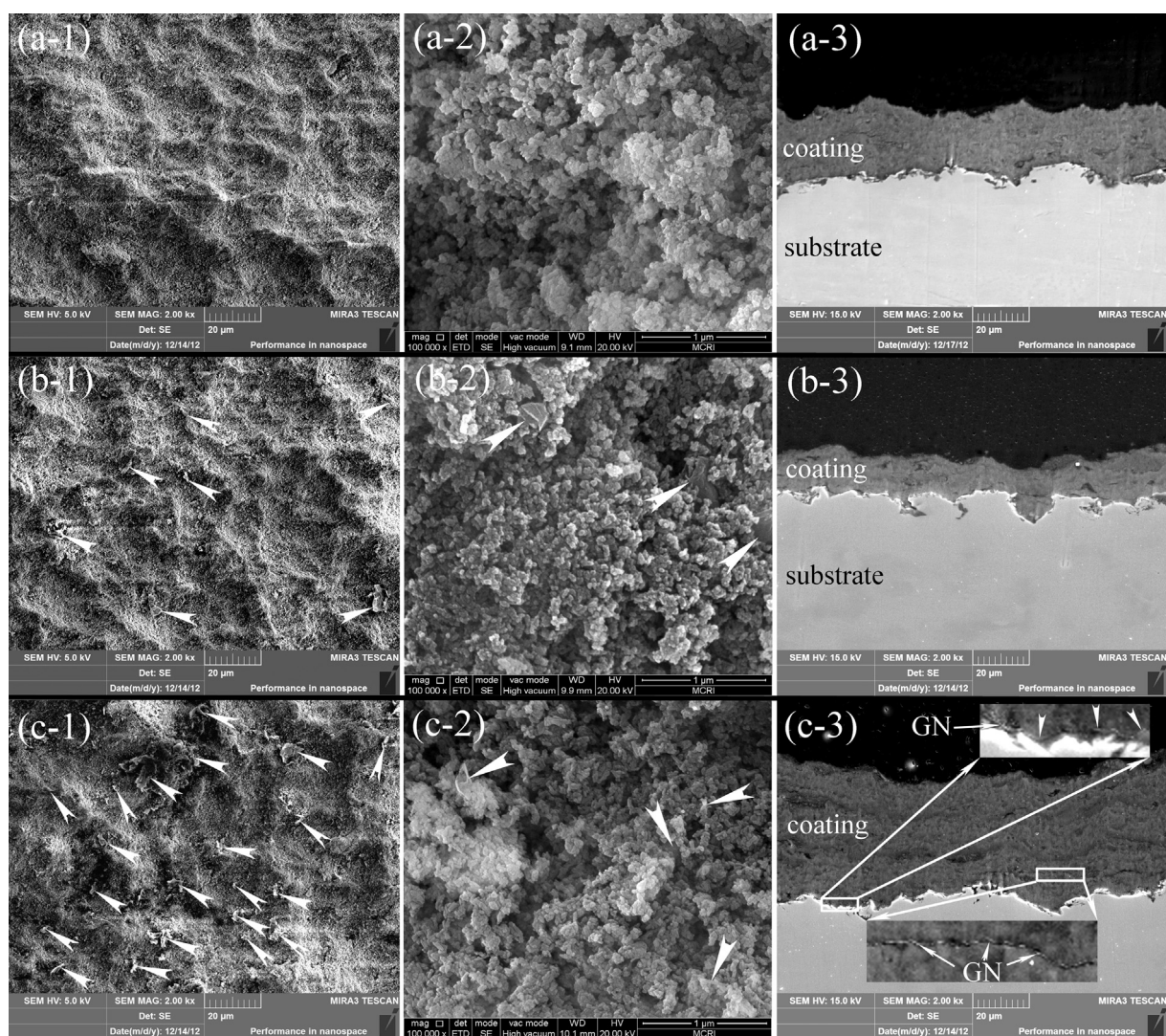


Fig. 2 – FESEM views of the as-deposited nanostructured coatings, (a) the pure HA coating, (b) the HA-0.1 wt.%GN coating, and (c) the HA-1.0 wt.%GN coating. -1: surface view, -2: magnified surface view, and -3: cross-sectional view. The white arrow head points to GN located on the surfaces of the coatings, and magnified views of typical areas from the cross-section of the HA-GN coating showing clearly the presence of GN in the coating and at the coating/substrate interface (c-3). GN-induced layered structure is clearly seen for the HA-GN coatings.

Unlike other surface coating techniques, VCS offers the advantages associated with room-temperature processing, for example, non-changes of phases in the coatings compared to the starting feedstock (Fig. 4a). Almost identical XRD peaks have been detected from the coatings and the feedstock powder. Of special interest is the intensity ratio of (300) peak to (002) peak of the VCS coatings, which increases dramatically in comparison with that of the starting powder, implying preferred crystallographic orientation of HA. This suggests possible grain breakage of individual starting nano particles upon their impingement on substrate/pre-coating [34,35]. Peak broadening attributed to the nano-sized crystal grains in the powder is retained and no new peaks for the as-sprayed coatings are seen. No detectable crystal grain growth is suggested.

3.2. Mechanical properties of the composite coatings

The adhesion of biomedical coating to substrate is one of the crucial factors that affect its long-term functional service after surgery [43]. In the current study, adhesive strength of the VCS coatings was assessed by the MST approach. During the MST test, when the diamond drill bit scratched the as-sprayed coatings, acoustic signal was acquired and was used to estimate the adhesion of the coatings. According to the acoustic emission vs critical load graphs for the coatings (Fig. 4b), the average normal force ranges from 20 to 45 N, showing irrelevance of adhesion to content of GN in the coatings. The theory behind the irrelevance is unknown yet, which needs further clarification. Nevertheless, the adhesion values are already higher than that of pulsed laser deposited

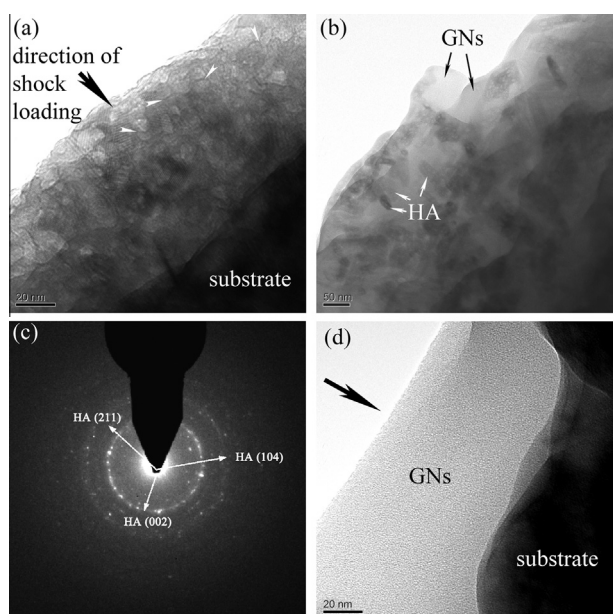


Fig. 3 – TEM images of the HA-1.0 wt.%GN coatings, (a) the image acquired at HA-rich area shows dense structure and plastic deformation of certain amount of the nano HA particles at their surrounding part of contact, (b) both GN and HA are clearly seen with intact structure as compared to the starting feedstock, and this is further verified by SAD pattern shown in (c), and (d) TEM image taken at coating/substrate interface suggests intimate contact of GN with the substrate.

HA coating on Ti-based implants, 10.77 N [44]. It is essential that the coatings can maintain the good adhesion in a physiological environment for a long term. In this study, no changes in adhesive strength were found for the coatings after 7 days *in vitro* incubation (with cells attaching on the coatings). In addition, one month incubation of the coatings in culture media without cells also showed no remarkable changes in the adhesion value. Assessment of fracture toughness of the coatings showed the K_{IC} value of $0.109 \pm 0.012 \text{ MPa m}^{1/2}$, $0.175 \pm 0.006 \text{ MPa m}^{1/2}$, and $0.421 \pm 0.011 \text{ MPa m}^{1/2}$ for the pure HA coating, the HA-0.1 wt.%GN coating and the

HA-1.0 wt.%GN coating, respectively. Apparently the presence of GN enhances the fracture property of the HA-based coatings. The toughening mechanisms of GN-containing ceramic bulk composites have been reported [17,38]. For the cold sprayed HA–GN composites, however, the toughening regimes might be different from the sintered ones, which need to be systematically investigated. VCS is believed to be an appropriate approach for depositing the HA–GN composites for favorable microstructure and promising mechanical properties.

3.3. *In vitro* biocompatibility of the composite coatings

Nontoxicity and favorable biocompatibility of the HA–GN composites are essentially required for their potential biomedical applications. To gain clear insight into effect of the addition of GN on cell responses, the cytotoxicity and biocompatibility of the HA–GN coatings were examined by MTT assay. Uncoated Ti samples were used as the control group for this experiment. SEM observation of the cells on the sample surfaces after the incubation time of 3 h, 1 day, 3 days, and 5 days suggests that the cells exhibit faster spreading and better stretching state on the HA-based coatings than on bare Ti (Fig. S1). And more GN in the HA-based coatings gave rise to faster recruitment of the cells. After 3 h incubation in the culture media, the percentage of the attached cells on the coatings increased statistically from 20% for the pure HA to 50% for the HA-0.1 wt.%GN and 80% for the HA-1.0 wt.%GN coatings. After 5 days incubation, the cells have reached confluent state on the HA-1.0 wt.%GN coating, whereas other samples were not fully covered by the cells yet. The HA-1.0 wt.%GN composite coating shows the highest cell proliferation rate (Fig. 5a), suggesting consistent results that GN enhances cell behaviors, apart from its exciting toughening effect on HA. In addition, further *in vitro* osteogenic differentiation was investigated by using ALP activity assay. The cells proliferated on the pure HA and the HA–GN composites had significantly higher ALP activity than those on the Ti plate. The ALP expression level on the HA-1.0 wt.%GN composites is about two times of that on the pure HA (16.6 U/g protein vs 7.9 U/g protein). The unobvious correlation between graphene dose and the changes in ALP activity could be attributed to

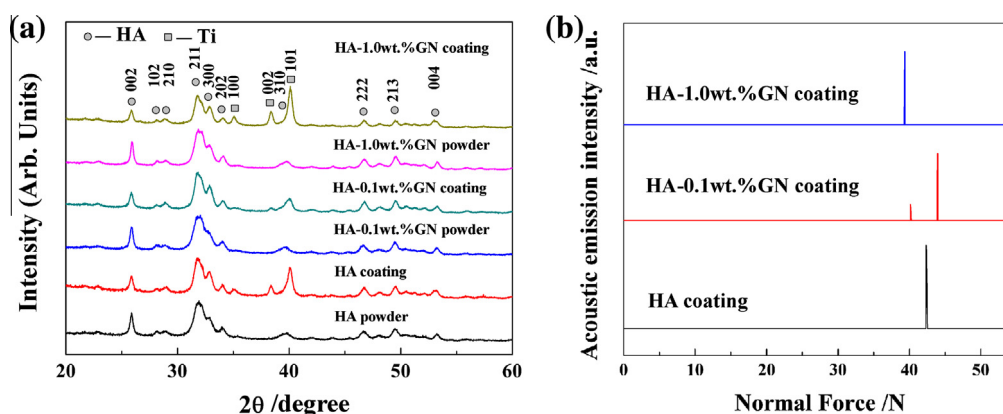


Fig. 4 – XRD spectra of the samples (a) (the detected Ti by the XRD analysis was from the substrate) and the adhesion testing results by measuring the normal force for the coatings (b). (A colour version of this figure can be viewed online.)

different differentiation states of the osteoblast cells. After 7 days of mineralization, the HA-1.0 wt.%GN coating was covered partly by flake-like Ca-P nanocrystals (Fig. S2), indicating that GN can serve as effective substrate for the nucleation of apatite crystals. Early cell spreading has been used as a model system for studying cell-extracellular matrix interactions [45], and it was revealed as a hydrodynamic process [46] and has been correlated to faster proliferation of cells [47]. The enhanced spreading of the cells on the GN-containing coatings possibly indicates more adhesion sites on the surfaces of the coatings. In fact, further examination of the spreading of the cells on the HA-GN coatings suggested preferential stretching of the cells to GN (Fig. 5b). Interestingly, it is noted that filopodia of the cells incline to approach GN, i.e. the filopodia extend primarily all the way to graphene sheet and get anchored by the sheet. It is noted that the direction of lateral filopodial movement is associated with that of cell migration [48] and in turn plays crucial roles in determining the fate of the cells. Even distribution of GN on the coating surfaces therefore favors elongation-adherence of the filopodia, consequently promoting spreading and proliferation of the cells. It was reported that F-actin supports finger-like protrusions of the plasma membrane filopodia [49]. And integrin receptors connect the extracellular matrix to actin cytoskeleton. This interaction can be viewed as a cyclical liaison, which develops again and again at new adhesion sites [50]. In this regard,

binding of integrin is crucial for modulating actin and consequent protrusions of filopodia.

It is established that upon contact of cells with biomaterials, selective and competitive adsorption of key serum proteins on biomaterial surface is the initial event participating in cell-biomaterial interactions. Attachment of cell is initiated by interaction of its integrins with pre-adsorbed serum proteins [51] and human osteoblasts adhere preferentially to fibronectin [52]. Fibronectin is a 450 kDa dimeric protein composed of homologous repeating structural motifs that are grouped together into functional domains [53]. Our TEM observation clearly shows fast adsorption of fibronectin on GN (Fig. 6a). After 2 h incubation, fibronectin was recruited by and attained entire adsorption on GN and showed an elongated conformation with the length of ~ 100 – 135 nm (Fig. 6b). The unfolded stretching state of GN infers that the arginine-glycine-aspartic acid (RGD) loop, the cell-binding site in type III domains of fibronectin [54], might have already been fully exposed for integrin-mediated cell binding. The early adsorption and stretching state of fibronectin presumably suggests that GN promotes its adsorption, which in turn facilitates attachment and spreading of the cells. Further investigation of adsorption of fibronectin on the HA-GN powder revealed preferred adsorption of fibronectin on GN (Fig. S3). Based on more than 200 TEM images acquired for each type of the samples, preliminary quantitative evaluation showed the adsorption rate of fibronectin to be 156 FN/ μm^2 on HA and 202 FN/ μm^2 on GN, which further proved preferred adsorption of fibronectin on GN. This agrees well with the phenomenon that GN at the coating surface promotes spreading and proliferation of the cells. Many factors affect the conformational changes of key serum proteins [55]. Enhanced adsorption of the proteins like vitronectin and fibronectin has been recognized on nanostructured materials as a result of the nanotexture or nanoroughness on their surfaces [30]. The micro-/nano-sized topographical features of the VCS HA-GN coatings (Fig. 2) are therefore anticipated to facilitate interaction with the proteins, leading to formation of a biomimetic structure. This biomimeticism may in turn promote the attachment of the osteoblast cells. It should be noted that the current study on protein adsorption is very preliminary, part of our ongoing efforts are devoted to investigating how the surface chemistry and morphology of the GN-containing coatings affect competitive adsorption and conformational changes of adsorbed multiple serum proteins and how the adsorbed proteins on their surfaces affect the cellular behaviors. In addition, recent studies already reported that higher specific surface area and surface-free energy of carbon composites increased cell density [56]. Faster attachment of osteoblast cells to the materials with greater nanometer surface roughness was reported [57]. The specific surface area of the VCS coatings showed the values of 35.6 , 42.3 , and 71.4 m^2/g for the pure HA coating, the HA-0.1 wt.%GN coating and the HA-1.0 wt.%GN coating respectively. The randomly curly GN brings about higher surface roughness and more active sites available for binding (Figs. 2c-1 vs a-1), likely facilitating preferential binding of the cells to the GN-containing coatings. We therefore propose that the HA-GN coatings possess good biological safety and noncytotoxicity and addition of GN enhances the behaviors of the cells. Compared with carbon nanotube-reinforced com-

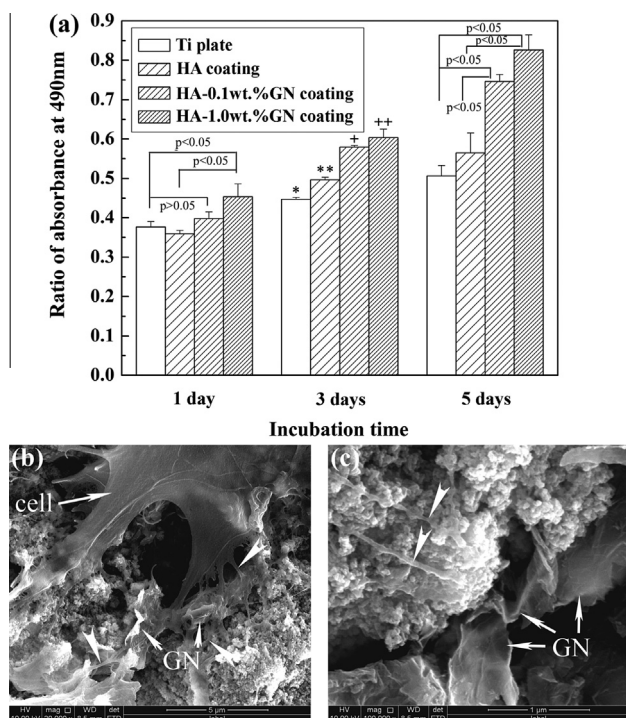


Fig. 5 – Cell culture results for the composite coatings, (a) MTT results for the cells proliferated on the surfaces of the coating samples, and (b, c) typical FESEM images showing preferential spreading of filopodia to and being anchored by GN present on the HA-1.0 wt.%GN coating surfaces, the white arrow heads point to filopodia of the cells. ++ vs *, ++ vs **, + vs *, + vs **: $p < 0.05$.

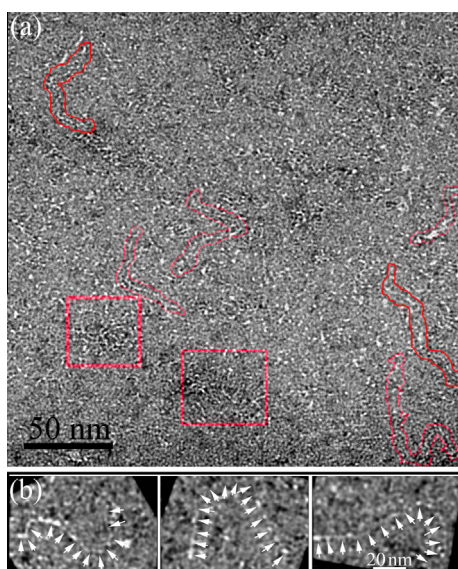


Fig. 6 – TEM images of fibronectin adsorbed on GN. (a) TEM image of the negative stained fibronectin on GN. Typical individual fibronectin molecule is surrounded by red line loop, while the areas enveloped by the red rectangular boxes show multiple fibronectin molecules tangling together. (b) Selected individual fibronectin molecules show the strands in coiled stretching state with the length of ~100–135 nm (the images were Gaussian low-pass filtered for clearer presentation of the molecule). The white arrows point to the molecule. (A colour version of this figure can be viewed online.)

posites, which bear the concern of harmful metallic impurities in carbon nanotubes [13,58,59], the HA–GN coatings have great promise as bioengineering materials due to the absence of metal catalysts during production of the graphene sheets [18–20,60].

4. Conclusions

We successfully deposited HA–GN composite coatings by VCS operated at room temperature. The coatings are uniform in tailorable thickness and showed competitive adhesive strength and fracture toughness. Comprehensive microstructural characterization showed that the physical characteristics of the starting feedstocks were completely inherited by the as-deposited coatings without detectable crystal grain growth or phase changes. GN was evenly embedded in HA matrix and plastic deformation of certain nano HA particles was revealed. The GN-containing HA coatings markedly enhanced attachment and proliferation of the osteoblast cells, which is most likely attributed to fast adsorption of key serum proteins like fibronectin with elongated stretching conformation on GN. The fabrication of the novel HA–GN composite biomedical coatings by the cold vacuum spray approach could open doors for processing new nanostructured biomaterials with exceptional properties.

Acknowledgements

This research was supported by National Natural Science Foundation of China (grant # 31271017) and 100 Talents Program of Chinese Academy of Sciences (both to H.L.).

Appendix A. Supplementary data

Supplementary data associated with this article can be found, in the online version, at <http://dx.doi.org/10.1016/j.carbon.2013.09.088>.

REFERENCES

- [1] Niinomi M. *Metallic biomaterials*. *J Artif Organs* 2008;11:105–10.
- [2] Sun LM, Berndt CC, Gross KA, Kucuk A. *Material fundamentals and clinical performance of plasma-sprayed hydroxyapatite coatings: a review*. *J Biomed Mater Res* 2001;58:570–92.
- [3] Kokubo T, Matsushita T, Takadama H. *Titania-based bioactive materials*. *J Eur Ceram Soc* 2007;27:1553–8.
- [4] Zitter H, Plenck Jr H. *The electrochemical behaviour of metallic implant materials as an indicator of their biocompatibility*. *J Biomed Mater Res* 1987;21:881–96.
- [5] Patterson SP, Daffner RH, Gallo RA. *Electrochemical corrosion of metal implants*. *Am J Roentgenol* 2005;184:1219–22.
- [6] Gu YW, Loha NH, Khor KA, Tor SB, Cheang P. *Spark plasma sintering of hydroxyapatite powders*. *Biomaterials* 2002;23:37–43.
- [7] Yu LG, Khor KA, Li H, Cheang P. *Effect of spark plasma sintering on the microstructure and in vitro behavior of plasma sprayed HA coatings*. *Biomaterials* 2003;24:2695–705.
- [8] Saber-Samandari S, Gross KA. *Amorphous calcium phosphate offers improved crack resistance: a design feature from nature?* *Acta Biomater* 2011;7:4235–41.
- [9] Velayudhan S, Anilkumar TV, Kumary TV, Mohanan PV, Fernandez AC, Varma HK, Ramesh P. *Biological evaluation of pliable hydroxyapatite–ethylene vinyl acetate co-polymer composites intended for cranioplasty*. *Acta Biomater* 2005;1:201–9.
- [10] Que W, Khor KA, Xu JL, Yu LG. *Hydroxyapatite/titania composites derived by combining high-energy ball milling with spark plasma sintering processes*. *J Eur Ceram Soc* 2008;28:3083–90.
- [11] Li J, Fartash B, Hermansson L. *Hydroxyapatite–alumina composites and none-bonding*. *Biomaterials* 1995;16:417–22.
- [12] Fu L, Khor KA, Lim JP. *Effects of yttria-stabilized zirconia on plasma-sprayed hydroxyapatite/yttria-stabilized zirconia composite coating*. *J Am Ceram Soc* 2002;84:800–6.
- [13] Zhang D, Yi C, Zhang J, Chen Y, Yao X, Yang M. *The effects of carbon nanotubes on the proliferation and differentiation of primary osteoblasts*. *Nanotechnology* 2007;18:475102–10.
- [14] Novoselov KS, Jiang D, Schedin F, Booth TJ, Khotkevich VV, Morozov SV, Geim AK. *Two-dimensional atomic crystals*. *Proc Natl Acad Sci USA* 2005;102:10451–3.
- [15] Stankovich S, Dikin DA, Dommett GHB, Kohlhaas KM, Zimney EJ, Stach EA, Piner RD, Nguyen ST, Ruoff RS. *Graphene-based composite materials*. *Nature* 2006;442:282–6.
- [16] Ramanathan T, Abdala AA, Stankovich S, Dikin DA, Herrera-Alonso M, Piner RD, et al. *Functionalized graphene sheets for polymer composites*. *Nat Nanotechnol* 2008;3:327–31.

- [17] Walker LS, Marotto VR, Rafiee MA, Koratkar N, Corral EL. Toughening in graphene ceramic composites. *ACS Nano* 2011;5:3182–90.
- [18] Chung C, Kim YK, Shin D, Ryoo SR, Hong BH, Min DH. Biomedical applications of graphene and graphene oxide. *Acc Chem Res* 2013. <http://dx.doi.org/10.1021/ar300159f>.
- [19] Wang Y, Li ZH, Wang J, Li JH, Lin YH. Graphene and graphene oxide: biofunctionalization and applications in biotechnology. *Trends Biotechnol* 2011;29:205–12.
- [20] Shen H, Zhang LM, Liu M, Zhang ZJ. Biomedical applications of graphene. *Theranostics* 2012;2:283–94.
- [21] Cook SD, Thomas KA, Dalton JE, Volkman TK, Whitecloud TS, Kay JF. Hydroxyapatite coating of porous implants improves bone ingrowth and interface attachment strength. *J Biomed Mater Res* 1992;126:989–1001.
- [22] Cook SD, Thomas K, Kay JE, Jarcho M. Hydroxyapatite coated titanium for orthopaedic implant applications. *Clin Orthop Relat Res* 1987;1232:225–43.
- [23] Geesink RGT, de Groot K, Klein CPAT. Chemical implant fixation using hydroxyapatite coatings. *Clin Orthop Relat Res* 1987;1225:147–70.
- [24] Klein CPAT, Patka P, Wolke JGC, Blicke-Hogervorst JMA, Groot K. Long term *in vivo* study of plasma sprayed coatings on titanium alloys of tetracalcium phosphate, hydroxyapatite, and t-tricalcium phosphate. *Biomaterials* 1994;15:146–50.
- [25] Heimann RB. Thermal spraying of biomaterials. *Surf Coat Tech* 2006;201:2012–9.
- [26] Tsui YC, Doyle C, Clyne TW. Plasma sprayed hydroxyapatite coatings on titanium substrates part 1: mechanical properties and residual stress levels. *Biomaterials* 1998;19:2015–29.
- [27] Tsui YC, Doyle C, Clyne TW. Plasma sprayed hydroxyapatite coatings on titanium substrates part 2: optimisation of coating properties. *Biomaterials* 1998;19:2031–43.
- [28] Webster TJ, Siegel RW, Bizios R. Osteoblast adhesion on nanophase ceramics. *Biomaterials* 1999;20:1221–7.
- [29] Gutwein LG, Webster TJ. Increased viable osteoblast density in the presence of nanophase compared to conventional alumina and titania particles. *Biomaterials* 2004;25:4175–83.
- [30] Webster TJ, Ergun C, Doremus RH, Siegel RW, Bizios R. Specific proteins mediate enhanced osteoblast adhesion on nanophase ceramics. *J Biomed Mater Res* 2000;51:475–83.
- [31] Webster TJ, Ergun C, Doremus RH, Siegel RW, Bizios R. Enhanced functions of osteoblasts on nanophase ceramics. *Biomaterials* 2000;21:1803–10.
- [32] Erickson HP, Carrell N, McDonagh J. Fibronectin molecule visualized in electron microscopy: a long, thin, flexible strand. *J Cell Biol* 1981;91:673–8.
- [33] Lima RS, Marple BR. Superior performance of high-velocity oxyfuel-sprayed nanostructured TiO₂ in comparison to air plasma-sprayed conventional Al₂O₃-13TiO₂. *J Therm Spray Techn* 2005;14:397–404.
- [34] Akedo J. Aerosol deposition method for fabrication of nano crystal ceramic layer-novel ceramics coating with collision of fine powder at room temperature. *Mater Sci Forum* 2004;449–452:43–8.
- [35] Akedo J. Room temperature impact consolidation (RTIC) of fine ceramic powder by aerosol deposition method and applications to microdevices. *J Therm Spray Techn* 2008;17:181–98.
- [36] Wang YY, Liu Y, Li CJ, Yang GJ, Kusumoto K. Electrical and mechanical properties of the nanostructure TiN coatings deposited by vacuum cold spray. *Vacuum* 2012;86:953–9.
- [37] Liu Y, Wang YY, Yang GJ, Feng JJ, Kusumoto K. Effect of nano-sized TiN additions on the electrical properties of vacuum cold sprayed SiC coatings. *J Therm Spray Techn* 2010;19:1238–43.
- [38] Liu Y, Huang J, Li H. Synthesis of hydroxyapatite-reduced graphite oxide composites for biomedical applications: oriented nucleation and epitaxial growth of hydroxyapatite. *J Mater Chem B* 2013;1:1826–34.
- [39] Anstis GR, Chantikul P, Lawn BR, Marschall DB. A critical evaluation of indentation techniques for measuring fracture toughness: I, direct crack measurements. *J Am Ceram Soc* 1981;64:533–8.
- [40] Ludtke SJ, Baldwin PR, Chiu W. EMAN: semiautomated software for high-resolution single-particle reconstructions. *J Struct Biol* 1999;128:82–97.
- [41] Gao PH, Li YG, Li CJ, Yang GJ, Li CX. Influence of powder porous structure on the deposition behavior of cold-sprayed WC-12Co coatings. *J Therm Spray Techn* 2008;17:742–9.
- [42] Viecek J, Gimeno L, Huber H, Lugscheider E. A systematic approach to material eligibility for the cold-spray process. *J Therm Spray Techn* 2005;14:125–33.
- [43] Duan Y, Zhu S, Guo F, Zhu J, Li M, Ma J, Zhu Q. The effect of adhesive strength of hydroxyapatite coating on the stability of hydroxyapatite-coated prostheses *in vivo* at the early stage of implantation. *Arch Med Sci* 2012;8:199–208.
- [44] Komath M, Rajesh P, Muraleedharan CV, Varma HK, Reshmi R, Jayaraj MK. Formation of hydroxyapatite coating on titanium at 200 °C through pulsed laser deposition followed by hydrothermal treatment. *Bull Mater Sci* 2011;34:389–99.
- [45] Giannone G, Dubin-Thaler BJ, Rossier O, Cai Y, Chaga O, Jiang G, et al. Lamellipodial actin mechanically links myosin activity with adhesion-site formation. *Cell* 2007;128:561–75.
- [46] Fardin MA, Rossier OM, Rangamani P, Avigan PD, Gauthier NC, Vonnegut W, et al. Cell spreading as a hydrodynamic process. *Soft Matter* 2010;6:4788–99.
- [47] Nelson CM, Chen CS. VE-cadherin simultaneously stimulates and inhibits cell proliferation by altering cytoskeletal structure and tension. *J Cell Sci* 2003;116:3571–81.
- [48] Xue F, Janzen DM, Knecht DA. Contribution of filopodia to cell migration: a mechanical link between protrusion and contraction. *Int J Cell Biol* 2010;2010:507821.
- [49] Zigmund SH. Signal transduction and actin filament organization. *Curr Opin Cell Biol* 1996;8:66–73.
- [50] Brakebusch C, Fässler R. The integrin-actin connection, an eternal love affair. *EMBO J* 2003;22:2324–33.
- [51] Pankov R, Cukierman E, Katz BZ, Matsumoto K, Lin DC, Lin S, et al. Integrin dynamics and matrix assembly: tensin-dependent translocation of alpha(5)beta(1) integrins promotes early fibronectin fibrillogenesis. *J Cell Biol* 2000;148:1075–90.
- [52] Gronthos S, Stewart K, Graves SE, Hay S, Simmons PJ. Integrin expression and function on human osteoblast-like cells. *J Bone Miner Res* 1997;12:1189–97.
- [53] Vogel V, Thomas WE, Craig DW, Krammer A, Baneyx G. Structural insights into the mechanical regulation of molecular recognition sites. *Trends Biotechnol* 2001;19:416–23.
- [54] Gee EPS, Yüksel D, Stultz CM, Ingber DE. SLLISWD sequence in the 10FNIII domain initiates fibronectin fibrillogenesis. *J Biol Chem* 2013. <http://dx.doi.org/10.1074/jbc.M113.462077>.
- [55] Stevens MM, George JH. Exploring and engineering the cell surface interface. *Science* 2005;310:1135–8.
- [56] Pesakova V, Kubies D, Hulejova H, Himmlöva L. The influence of implant surface properties on cell adhesion and proliferation. *J Mater Sci Mater Med* 2007;18:465–73.
- [57] Price RL, Ellison K, Haberstroh KM, Webster TJ. Nanometer surface roughness increases select osteoblast adhesion on carbon nanofiber compacts. *J Biomed Mater Res A* 2004;70:129–38.
- [58] Kalbacova M, Kalbac M, Dunsch L, Hempel U. Influence of single-walled carbon nanotube films on metabolic activity

-
- and adherence of human osteoblasts. *Carbon* 2007;45:2266–72.
- [59] Liu Z, Tabakman S, Welsher K, Dai HJ. Carbon nanotubes in biology and medicine: *in vitro* and *in vivo* detection, imaging, and drug delivery. *Nano Res* 2009;2:85–120.
- [60] Mcallister MJ, Li JL, Adamson DH, Schniepp HC, Abdala AA, Liu J, et al. Single sheet functionalized graphene by oxidation and thermal expansion of graphite. *Chem Mater* 2007;19:4396–404.